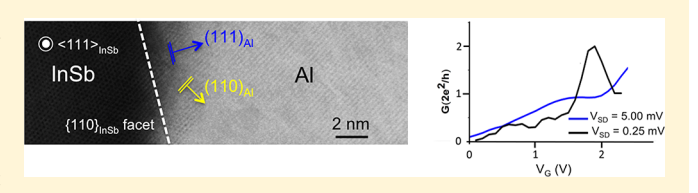
Downloaded via UNIV ILLINOIS URBANA-CHAMPAIGN on August 18, 2020 at 17:34:15 (UTC). See https://pubs.acs.org/sharingguidelines for options on how to legitimately share published articles.

# Selective-Area Superconductor Epitaxy to Ballistic Semiconductor **Nanowires**

Stephen T. Gill,\*\*,<sup>†</sup> Jeff Damasco,<sup>†</sup> Blanka. E. Janicek,<sup>‡</sup> Malcolm S. Durkin,<sup>†</sup> Vincent Humbert,<sup>†</sup> Sasa Gazibegovic,<sup>§,||</sup> Diana Car,<sup>§,||</sup> Erik P. A. M. Bakkers,<sup>§,||</sup> Pinshane Y. Huang,<sup>‡</sup> and Nadya Mason\*\*,<sup>†</sup>

Supporting Information

ABSTRACT: Semiconductor nanowires such as InAs and InSb are promising materials for studying Majorana zero modes and demonstrating non-Abelian particle exchange relevant for topological quantum computing. While evidence for Majorana bound states in nanowires has been shown, the majority of these experiments are marked by significant disorder. In particular, the interfacial inhomogeneity between



the superconductor and nanowire is strongly believed to be the main culprit for disorder and the resulting "soft superconducting gap" ubiquitous in tunneling studies of hybrid semiconductor-superconductor systems. Additionally, a lack of ballistic transport in nanowire systems can create bound states that mimic Majorana signatures. We resolve these problems through the development of selective-area epitaxy of Al to InSb nanowires, a technique applicable to other nanowires and superconductors. Epitaxial InSb-Al devices generically possess a hard superconducting gap and demonstrate ballistic 1D superconductivity and near-perfect transmission of supercurrents in the single mode regime, requisites for engineering and controlling 1D topological superconductivity. Additionally, we demonstrate that epitaxial InSb-Al superconducting island devices, the building blocks for Majorana-based quantum computing applications, prepared using selective-area epitaxy can achieve micron-scale ballistic 1D transport. Our results pave the way for the development of networks of ballistic superconducting electronics for quantum device applications.

KEYWORDS: Epitaxy, ballistic transport, nanowires, supercondivity, indium antiminoide, aluminum

Semiconductor nanowire (NW) systems have captured great attention because of their potential use in novel great attention because of their potential use in novel quantum devices. 1-4 Recently, topological superconductivity harboring Majorana bound states has become a global pursuit in semiconductor nanowires.<sup>5,6</sup> While preliminary experimental work demonstrated signature zero-bias conductance peaks, 7-10 the devices also demonstrated significant disorder. One notable feature was significant subgap conductance in the tunneling spectroscopy of the induced superconducting gap in the nanowire. 7-10 The so-called soft gap, which is believed to result from an inhomogeneous semiconductor-superconductor interface, 11 has been resolved using molecular-beam epitaxy (MBE) techniques to grow epitaxial Al on InAs<sup>12</sup> and InSb<sup>13</sup> nanowires. However, such techniques are costly and not widely available to the community. In contrast, ex situ processing, in which metallization and wire fabrication occur in separate steps, can produce uniform interfaces and a hard superconducting at a zero magnetic field. 14,15 The growth of superconductors with suitable critical magnetic fields using conventional deposition techniques has been limited to highly disordered NbTiN<sup>16</sup> to date. 15 Besides disorder, NbTiN has the drawback of the development of a soft gap at finite

magnetic field from vortex entry, which prevents the application to topological superconducting devices. 15,17 In contrast, nanowires with thin aluminum shells maintain robust superconductivity to roughly 2 T,18 a result of the well-known property that thin Al (thickness of ≤10 nm) can survive in large magnetic fields. 19 Therefore, replacing NbTiN with epitaxial Al films of thickness less than 10 nm using conventional deposition techniques can provide a significant breakthrough for accessing and the scaling up of topological superconductity in nanowires and nanowire networks. 13,2

In this work, we present selective area epitaxy of Al to InSb nanowires and demonstrate the high-quality electron transport enabled by epitaxial interfacing. The facets of the wire are kept sharply intact after removing the oxide using sulfur-based etching<sup>21</sup> while providing a low-roughness surface for epitaxial growth, as shown in Figure 1A. By the engineering of a clean surface without damaging the InSb crystal, Al grows epitaxially to InSb, as shown in Figure 1B, for low-temperature electron-

Received: April 17, 2018 Revised: August 17, 2018 Published: September 10, 2018



<sup>&</sup>lt;sup>†</sup>Department of Physics and <sup>‡</sup>Department of Materials Science and Engineering, University of Illinois at Urbana—Champaign, Urbana, Illinois 61801, United States

<sup>&</sup>lt;sup>§</sup>QuTech and Kavli Institute of NanoScience, Delft University of Technology, 2600 GA Delft, The Netherlands

Department of Applied Physics, Eindhoven University of Technology, 5600 MB Eindhoven, The Netherlands

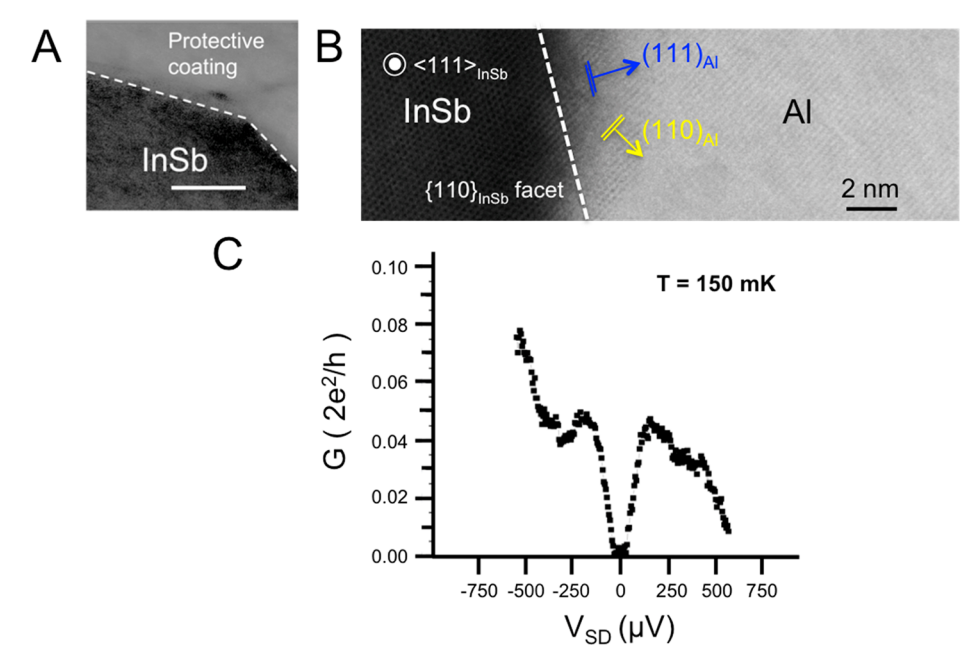


Figure 1. Low-disorder interface and epitaxy of ln Sb—Al nanowires: (A) Cross-sectional bright-field scanning transmission electron microscopy (BF-STEM) image of an InSb nanowire surface cleaned by a sulfur-based etching and brief Ar ion mill. A metal capping layer was deposited as a protective coating before STEM imaging to protect the interface from oxidizing. A smooth interface is left on the top facet, and the etching does not degrade the original faceting of the nanowire. The white scale bar is 10 nm. (B) Cross-sectional STEM image taken with the InSb nanowire aligned along its <111> zone axis (indicated by the dotted circle), showing the epitaxial contacting between Al and InSb following optimized etching and deposition. The white dashed line marks the InSb {110} facet. In the Al region of the STEM image, streaking is from the (110) planes of Al (double yellow lines are superimposed on these planes) growing in-plane along the nanowire's growth direction. (111) planes of Al are drawn as blue lines to indicate the out-of-plane growth orientation. Arrows indicate the normal vectors to the Al (110) and (111) lattice planes. The cross-section is taken from the nanowire device shown in Figure 3A. (C) Tunneling conductance of a normal-superconducting (NS) device geometry as a function of source-drain voltage demonstrating a hard induced superconducting gap.

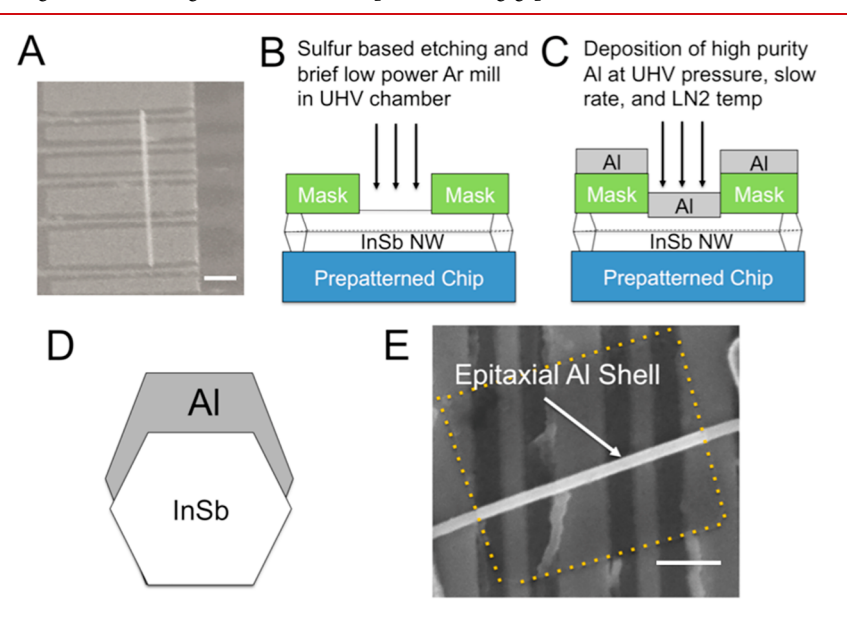


Figure 2. Schematic of processing for patterned epitaxy: (A) SEM image of an InSb nanowire transferred to a pre-patterned chip with local gate electrodes. The scale bar is 750 nm. (B) Schematic of surface cleaning for preparing clean InSb surfaces. Nanowires are patterned with masks using e-beam lithography. The mask is used to selectively etch and clean the nanowire using sulfur passivation and ion milling. (C) Schematic of deposition conditions required for epitaxial growth. (D) Illustration of the general growth of Al onto InSb in our system. The deposition source is located 1 m away from the sample, so the growth is highly directional, and Al grows dominantly on the top facet. (E) SEM image of a completed deposition where a nominal 8 nm epitaxial Al shell is left on the nanowire. The yellow dashed lines outline the mask that was used to etch and selectively grow Al on the nanowire. The scale bar is 200 nm.

beam deposition in ultrahigh-vacuum (UHV) conditions. The Al generically induces a hard superconducting gap in the nanowire, as shown in Figure 1C, also confirming the low-

disorder interfacing. We also report on low-temperature transport measurements for epitaxial InSb-Al devices that demonstrate superlative transport features such as the near-

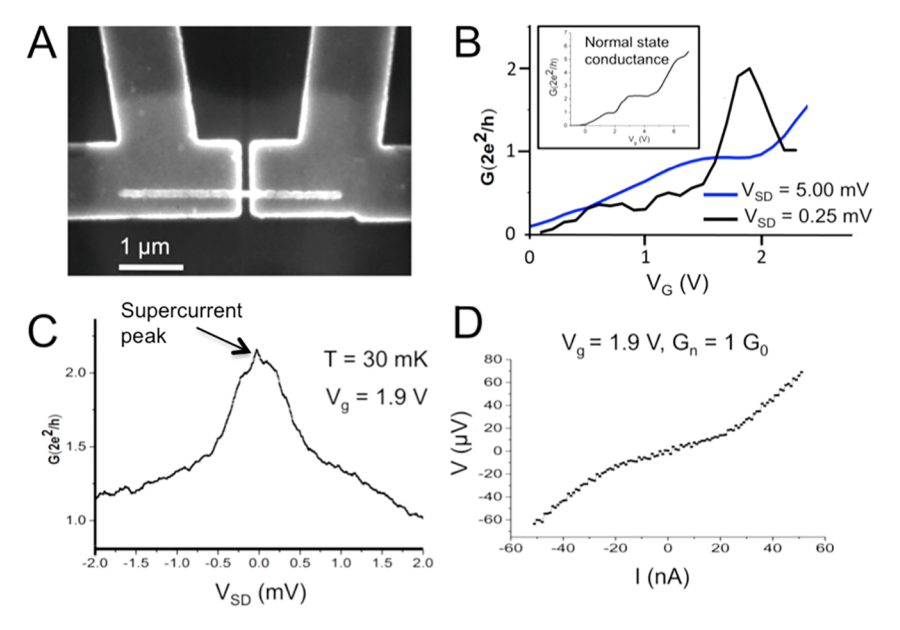


Figure 3. Andreev doubling and transparent transmission of Cooper pairs through an exitaxial Al–lnSb–Al junction: (A) SEM image of an Al–lnSb Josephson junction whose epitaxial interfacing is shown in Figure 1B. (B) Differential conductance as a function of gate voltage  $V_G$  at  $V_{SD} = 2\Delta_0 = 250~\mu\text{V}$ , i.e., single Andreev reflection conductance, (black line) and at  $V_{SD} = 5~\text{mV} \gg 2\Delta_0$  (blue line), where the device is normal. On a resonance value of  $V_G = 1.9~\text{V}$ , the Andreev conductance nearly doubles from the normal-state value, as expected for a pristine interface. Inset shows normal conductance quantization for the device. (C) Differential conductance as a function of source-drain voltage of the device on the resonant gate voltage of  $V_G = 1.9~\text{V}$ . For  $V_{SD} < 2\Delta_0$ , the device conductance rises above twice the normal-state conductance, signaling SNS behavior. Small offset of the peak from  $V_{SD} = 0~\text{mV}$  is from an instrument offset. (D) IV behavior of the device on resonance showing a switching current of roughly 24 nA.

unity transmission of Andreev reflection and micron-scale ballistic transport. These results suggest that selective area epitaxy of InSb—Al nanowires is a promising system for controlling mesoscopic superconductivity and is particularly relevant for nanowire-based superconducting quantum computation (i.e., Andreev qubits<sup>22</sup> and gatemons<sup>23</sup>).

First, we discuss the procedure for selective area epitaxy of Al to InSb nanowires. Fabrication begins by depositing nanowires on a prepatterned chip with a micromanipulator. See the Supporting Information for additional details regarding chip preparation. A transferred wire is shown in Figure 2A. Next, we use conventional electron-beam lithography for masks in all etching and deposition steps, as schematically demonstrated in Figure 2B,C. To remove the native oxide, a key step for preparing a transparent interface, we use sulfur passivation as a first step in surface cleaning. 21 Following sulfur passivation, the sample is transferred to a load-locked UHV system in which the chip is outgassed for several hours until base pressure of the load lock chamber is achieved. After the outgassing of the chip, a brief, low-energy Ar ion mill is performed to remove any adsorbates on the nanowire surface. As evidenced in Figure 1A,B, this processing produces a nearly disorder-free surface where there is no visible amorphous layer at the surface of the nanowire. Indeed, recent work has shown that via the optimization of sulfur-based etching, low-disorder InSb nanowire interfaces can be prepared for depositing superconductors and inducing a hard gap comparable to the gap "hardness" demonstrated in MBE-based InAs-Al nanowires. 14,15 However, this work on ex situ based superconductor deposition required a disordered sticking metal, such as NbTi or Ti, and there was non-epitaxial growth of the parent superconductor to achieve a hard gap. In that case, it was not possible to interface the nanowire with Al, which was attributed to non-epitaxial growth. <sup>14</sup> Similarly, we have deposited Al at room temperature onto InSb nanowires using similar procedures as in ref 14 and have measured contact resistances on the order of  $M\Omega$ s.

We now outline the conditions required for selective area epitaxy of Al following surface preparation, which is schematically represented in Figure 2C. The growth occurs at liquid nitrogen temperature with a low background pressure of  $\sim 1.5-4 \times 10^{-10}$  Torr during the cooling and before deposition. Once the sample is at liquid nitrogen temperature, high-purity Al is electron-beam-evaporated. In our growth procedure, Al films are deposited at a rate of ~0.1 A/s. The Al flux is linearly directed at the sample, as illustrated in Figure 2C,D. Scanning transmission electron microscopy (STEM) characterization of a typical device reveals areas of epitaxial interfacing, as shown in Figure 1B. The TEM image, taken where the InSb nanowire is aligned along the <111> zone axis, shows the Al (110) planes growing in plane to the top InSb {110} facet. The Al (110) planes seen along the <111> orientation are a result of Al (111) growth out of plane to the <111> nanowire growth direction. As pointed out in Krogstrup et al., 12 the low temperature is critical for achieving crystalline thin films of a single grain where minimizing surface free energy is the dominant mechanism for determining the out of plane crystal orientation. For FCC metals such as Al, the lowest-surface-energy orientation is generally (111). Hence, our TEM analysis confirms we are growing epitaxial Al films where surface free-energy minimization is the strongest thermodynamic driver in dictating the film's out of plane crystallinity. After deposition and a several-hour-long warming to room temperature, a standard liftoff in acetone is used to remove resist, and, as shown in Figure 2E, a smooth film of Al is left on the nanowire. Our growth conditions reproducibly result in the growth of a continuous, smooth Al shell onto InSb. In contrast to the elevated temperature growth of

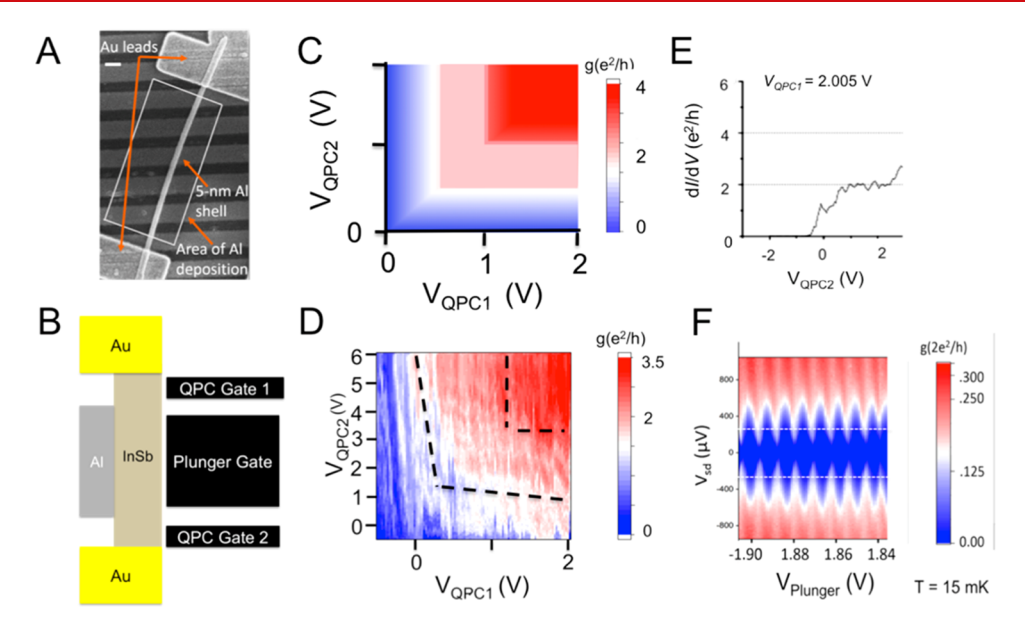


Figure 4. Micron-scale ballistic transport and engineered confinement in an exitaxial ln Sb–Al device. (A) SEM image of a representative epitaxial InSb–Al island device. An Al island of thickness below 10 nm is deposited selectively between two gold leads. Local gates tune the QPC in the bare regions between the leads and island, and a plunger gate tunes the chemical potential under the proximitized InSb nanowire. The white scale bar is 200 nm. (B) Schematic of the epitaxial InSb–Al island device. A pair of gates acting as QPCs in the bare constrictions between Au leads control the device from Coulomb blockaded to ballistic quantum wire regimes. A plunger gate is used to tune the chemical potential in the epitaxial InSb–Al nanowire. (C) Schematic of the conductance as a function of arbitrary gate voltage on two series QPCs when transport through a reservoir is ballistic according to Landauer's formula.<sup>42</sup> The conductance is dominated by plateaus indicating how many modes are transmitting. (D) Conductance as a function of two series QPCs in a 600 nm island device (Al thickness of 5 nm) when the plunger is grounded. As highlighted by the dashed lines, conductance is dominated by the quantized conductance plateau for single mode transmission, indicating quantum addition and ballistic transport of a single mode through the InSb–Al island. Note that a 1 mV bias was applied to suppress superconductivity. (E) Line trace from the conductance map in panel D for the gate voltage on QPC 1 held at  $V_{\rm QPCI} = 2.005$  V. A robust quantized conductance plateau is seen with minor fluctuations imposed, indicating ballistic transmission of a single mode through the InSb–Al island. (F) Map of differential conductance as a function of source-drain voltage and plunger voltage showing Coulomb blockade. Both QPC gates are held at -0.45 V to deplete the QPC. The superconducting gap is  $\Delta_0 = 250 \ \mu eV$ , and the charging energy is 350  $\mu eV$ .

epitaxial Al on InAs,<sup>24</sup> we do not observe out of plane variations, which would indicate polycrystalline growth along the nanowire growth direction. As discussed above, the lack of out-of-plane variations is a result of the low-temperature growth promoting a large area grain along the nanowire having a single out-of-plane crystal orientation.

The surface homogeneity of the nanowire-superconductor surface and the crystalline superconducting film enables the superconductor to impart a hard superconducting density of states in the nanowire. As shown in Figure 1C, the tunneling regime of a ballistic normal-superconductor (NS) nanowire device shows strong suppression of conductance below the superconducting gap. In particular, the measured ratio of zerobias conductance  $(G_{V=0})$  to normal-state conductance  $(G_N)$  in this device reveals a suppression of  $G_{V=0}/G_N$  < 1/50, comparable to gap hardness in MBE-based Al-InAs nanowires. 25,26 In addition to strong suppression of subgap conductance in the tunneling regime, we find that the device, which is coupled to a quantum point contact (QPC), achieves a large zero-bias Andreev enhancement to 1.7  $G_0$  in the single mode regime of the QPC (see the Supporting Information), implying 96% transmission. 14,25,26 Furthermore, a 2D map of conductance as a function of gate and source-drain voltage reveals the device evolves from tunneling to the single mode regime without localization features, also consistent with highly transparent leads (see the Supporting Information).

We now discuss the high-quality ballistic 1D superconductivity that can be achieved in our epitaxial InSb-Al nanowires. In particular, we focus on the transparency of the epitaxial InSb-Al nanowire interface in the single mode regime, which is relevant for engineering Majorana modes. 5,6 As we have demonstrated previously, InSb nanowires interfaced with Al can be engineered to have a quantum point contact response (i.e., quantization of conductance steps), which allows gate voltage tuning to the single mode regime.<sup>27</sup> Figure 3A shows an Al-InSb-Al nanowire Josephson junction where quantized transport of the normalstate conductance is observed, as shown in the inset of Figure 3B. (See the Supporting Information for detail regarding the device fabrication). The main part of Figure 3B shows that the first quantized conductance plateau, at  $\sim 2e^2/h$ , is enhanced in the superconducting regime to  $\sim 4e^2/h$ . This enhancement is caused by Andreev reflection, the process of generating superconducting proximity effect by an electron reflecting as a hole at the nanowire-superconductor interface.<sup>28</sup> For pristine superconducting-normal interfaces, a single Andreev reflection can enhance conductance by a factor of 2.<sup>28</sup> In SNS systems, the cross-over from Andreev to normal conductance occurs at  $eV_{SD} = 2\Delta_0$ , where  $\Delta_0$  is the induced gap in the proximitized region and the factor of 2 accounts for two S-N interfaces in series. For the device in Figure 3, we observe a resonant superconducting behavior in which the conductance closely reaches the theoretical limit of  $4e^2/h$  at  $eV_{SD} = 2\Delta_0$ indicating a near unity Andreev reflection probability at the

interface, when the normal conductance is tuned to the middle of the single mode conductance plateau. Figure 3C shows the bias dependence on resonance where a strong Andreev conductance enhancement to 4e<sup>2</sup>/h and above is observed in the cross-over from normal to Andreev conductance,  $V < 2\Delta_0$ , where  $\Delta_0 = 125 \mu \text{eV}$  is the induced gap in the proximitized region from the Ti/Al leads. While the presence of multiple Andreev resonances is typically presented to imply a transparent interface, we note that the disappearance of these resonances is expected for the zero-scattering and lowtemperature limit of multiple Andreev reflection theory.<sup>29–31</sup> Additionally, enhanced conductance above 2e<sup>2</sup>/h for small voltages above  $eV_{SD} = 2\Delta_0$  is from excess current, <sup>28</sup> which we have observed before in superconducting InSb QPCs.<sup>27</sup> Note the small zero bias peak imposed on the broader enhanced Andreev conductance is due to a supercurrent. An 8  $\mu$ V excitation was used in the differential conduction measurement, which suppresses the magnitude of the zero-bias peak from the supercurrent. When the device is further opened with the backgate to allow additional modes, Andreev transport becomes sharply suppressed. Similar resonant Andreev enhancement behavior has been observed in InSb nanowires and in QPC formed in epitaxial InAs-Al 2DEGs.32

The transparent InSb-Al interface is also evident from the switching current measured when the device is tuned to resonant Andreev transport. Given the resonant Andreev behavior, we observe switching current resonances rather than plateaus, consistent with the correlation of Andreev transport to switching currents (see the Supporting Information). Figure 2D shows a switching current of  $I_S \approx 24$  nA when the device is tuned to the gate voltage where Andreev doubling appears. We note that the residual resistance (less than 1  $k\Omega$  and more than a factor of 10 smaller resistance than the normal-state resistance) observed below the switching current,  $I_{S,r}$  is from phase diffusion in a small, unshunted junction 33,34 and is commonly observed when the normal-state resistance is large. 35,36 The switching current for a perfect S-QPC-S junction at unity transmission is given by  $I_N = 2\pi Ne\Delta_0/h$ , where N is the number of modes and  $\Delta$  is the induced superconducting gap.<sup>37</sup> For a gap of 125  $\mu$ eV, the maximum supercurrent for a single mode weak link would be 30 nA. Accounting for the deviation from an ideal junction by finite reflections, 38 we extract a transmission of 96%. Consideration of thermal suppression would lead to an even higher transmission value, 33,38,39 consistent with having achieved a nearly pristine epitaxial interface. We have measured similar behavior in multiple other devices, indicating that pristine interfaces can be achieved reproducibly and that epitaxial Al-InSb NW Josephson junctions can demonstrate nearly ideal mesoscopic superconductivity.

Next, we demonstrate that not only is transport ballistic in the QPC formed in the bare nanowire between contacts but that the epitaxial Al–InSb NW segment is also a ballistic quantum wire. One of the major developments enabled by the growth of epitaxial Al–InAs nanowires was the development of gate tunable superconducting islands for studying 1D topological superconductivity, i.e., the so-called Majorana island geometry. We focus on the behavior of epitaxial InSb–Al nanowires in the island geometry, with a device and schematic shown in Figure 4A,B. We note that the devices tested had a single plunger gate under the superconducting shell. Thin gates underneath the bare nanowire form quantum point contacts coupling the epitaxial InSb–Al nanowire to the

leads. For two QPCs in series to a ballistic reservoir, the resistance is modulated as  $R_{\text{Tot}} = \text{Max}(R_{\text{QPC1}}, R_{\text{QPC2}})$ . In contrast, a diffusive reservoir's conduction would be modulated by Ohmic addition  $(R_{\text{Tot}} = R_{\text{QPC1}} + R_{\text{QPC2}} + R_{\text{inelastic}})^{42}$ . The plot in Figure 4C is of a schematic of the expected behavior for the conductance for two quantum point contacts in series with a ballistic reservoir. The plot on the right in Figure 4D shows the response of a 600 nm long epitaxial InSb-Al quantum wire (5 nm epitaxial film of aluminum) coupled to two 200 nm long quantum point contacts. For this measurement the plunger gate is grounded and a finite voltage is applied to drive the device normal. We see that the conductance in this device shows behavior corresponding to quantum addition where the conductance is dominated by the plateau behavior of the QPCs. As shown in Figure 4E, a cut from the plot shows a robust plateau at  $dI/dV = 2e^2/h$ , with small mesoscopic fluctuations imposed, indicating ballistic, single-mode transport. The quantization quality is comparable to what is seen in long quantum wires. 43,44 This transport behavior demonstrates that there is ballistic transport through the Al-InSb NW portion and that there is QPC coupling of the superconducting NW to the leads. Hence, electrons are traveling more than a micron without scattering in these structures. Even more importantly, the data suggests the NW has been tuned into a regime in which there is, most likely, a single mode flowing in the semiconductor-superconductor NW, realizing the required single-mode quantum wire regime to engineer Majorana zeromodes and observe helical transport.

In the tunnel-coupled limit, the device operates as an isolated superconducting island in the Coulomb blockade regime. The epitaxy technique enables the use of very thin films (we use <10 nm Al for islands) that can be strongly gated to tune the proximitized nanowire. Figure 3D shows the Coulomb blockade behavior of the InSb-Al NW from Figure 3C when the QPC gates are tuned to pinch off. The plunger gate modulates the single electron Coulomb blockade with a periodicity of roughly 7 mV and with an extracted charging energy of 350  $\mu$ eV, giving a lever arm of  $\eta = 0.05$  eV/V, indicating strong coupling of the plunger to the proximitized nanowire. This result indicates the extra metal deposited in the epitaxial contacting to the nanowire does not significantly screen the gate. We note that connecting the additional metal deposited in the epitaxial contacting of the nanowire to the plunger can enhance the plunger coupling (i.e., decrease the charging energy). This is relevant for tuning the superconducting island to a regime in which  $\Delta_0 > E_C$  in order to observe 2e periodic Coulomb blockade and measure the topological transition to 1e periodic Coulomb blockade from electron "teleportation" by means of Majorana zero modes. 41 Our ability to strongly tune the chemical potential of the superconducting quantum wire will allow us, in future experiments, to explore the topological phase diagram of InSb-Al nanowires and the signature of exponential protection in the Majorana island geometry.

While our epitaxial growth procedure is applicable to other nanowire systems (e.g., InAs nanowires), epitaxial InSb–Al NWs offer several advantages for studying topological superconductivity over other NW systems. For example, the g factor of InSb is roughly a factor of 5–10 larger than in InAs NWs, 15,45–47 significantly reducing the required magnetic field to enter the topological regime. Additionally, InAs nanowires, including the epitaxial Al–InAs system, are prone to developing unintentional quantum confined regions from

surface sensitivity in InAs. 18,48 For the epitaxial InAs-Al system, device fabrication requires a harsh etch to remove unwanted Al, which results in random quantum-dot formation. 18 Indeed, signatures of Majorana in these devices show zero-energy bound states with spectral weights far below the expected quantized values and broadening inconsistent with the Majorana interpretation despite the improved proximity superconductivity. 40 These results suggest that disorder is still playing a large role in the readout of Majorana zero-modes and that quantum control in the system is lacking. However, InSb nanowires devices can be ex situ processed to give a full yield of devices showing ballistic 1D transport, as evidenced by robust quantized conductance at zero-magnetic field and miliKelvin temperatures. 15,27,49 We note that the InSb–Al system has never yielded unintentional Coulomb blockaded, quantum dot-like transport. In particular, we have measured Andreev enhancement and switching current correlation to the normal-state conductance quantization in approximately 20 devices. We note that the observation of approximate Andreev doubling and switching currents approaching the quantized limit has only been observed in several devices because this requires high-quality normal-state conductance quantization and, hence, extremely clean wires. We believe such high-quality ballistic devices should show rich behavior in a magnetic field. In particular, future measurements will test the behavior of the induced gap of thin Al shell devices in magnetic field to perform quantum point contact spectroscopy experiments of Majorana states.50

In conclusion, we have presented selective area superconductor epitaxy to semiconductor nanowires. In particular, we have focused this technique on InSb nanowires to develop superconducting quantum wires. We have demonstrated that epitaxial growth of Al following sulfur-based removal of the native oxide results in a nearly ideal superconducting interface. As a result of this clean interface, we realize near-unity Andreev reflection at the InSb-Al interface, which gives large conductance enhancements from Andreev reflection and nearly unity transmission of supercurrents in the single mode regime. In addition, we have shown that this method is amenable to developing ballistic superconducting island devices with QPC coupling to the leads. Our quantum point contact control in InSb-Al nanowires should enable proper determination of the topological transition<sup>51</sup> and further establish epitaxial InSb-Al nanowires as a promising platform for studying and manipulating Majorana modes.

## ASSOCIATED CONTENT

#### S Supporting Information

The Supporting Information is available free of charge on the ACS Publications website at DOI: 10.1021/acs.nanolett.8b01534.

Details of the fabrication, the measurement setup, TEM imaging, and the treatment of contact and series resistance along with extended data and discussion for the devices in Figures 1–4. (PDF)

### AUTHOR INFORMATION

#### **Corresponding Authors**

\*E-mail: gill15@illinois.edu. \*E-mail: nadya@illinois.edu.

ORCID ®

Stephen T. Gill: 0000-0001-9720-3776

Diana Car: 0000-0002-6371-8285

Erik P. A. M. Bakkers: 0000-0002-8264-6862

#### Notes

The authors declare no competing financial interest.

#### ACKNOWLEDGMENTS

S.T.G, J.D., and N.M. were supported by the Office of Naval Research, grant no. N0014-16-1-2270. J.D and V.H. acknowledge support from NSF DMR-1710437 and M.S.D acknowledges support from DOE SE-SC0012649. B.E.J. and P.Y.H. were supported by the Office of Naval Research, grant no. N00014-16-1-2436. S.G., D.C., and E.P.A.M.B. were partly supported by the European Research Council and The Netherlands Organization for Scientific Research. S.T.G acknowledges support from an NSF Graduate Research Fellowship. S.T.G, J.D., B.E.J., M.S.D., V.H., P.Y.H, and N.M. acknowledge the use of the Materials Research Lab Central Facilities at the University of Illinois for all work.

#### REFERENCES

- (1) Nadj-Perge, S.; Frolov, S. M.; Bakkers, E. P. A. M.; Kouwenhoven, L. P. Spin-Orbit Qubit in a Semiconductor Nanowire. *Nature* **2010**, *468*, 1084–1087.
- (2) Petersson, K. D.; McFaul, L. W.; Schroer, M. D.; Jung, M.; Taylor, J. M.; Houck, A. A.; Petta, J. R. Circuit Quantum Electrodynamics with a Spin Qubit. *Nature* **2012**, *490*, 380–383.
- (3) Liu, Y.-Y.; Stehlik, J.; Eichler, C.; Gullans, M. J.; Taylor, J. M.; Petta, J. R. Semiconductor Double Quantum Dot Micromaser. *Science* **2015**, 347, 285–287.
- (4) Hofstetter, L.; Csonka, S.; Nygård, J.; Schönenberger, C. Cooper Pair Splitter Realized in a Two-Quantum-Dot Y-Junction. *Nature* **2009**, *461*, 960–963.
- (5) Lutchyn, R. M.; Sau, J. D.; Das Sarma, S. Majorana Fermions and a Topological Phase Transition in Semiconductor-Superconductor Heterostructures. *Phys. Rev. Lett.* **2010**, *105*, 077001.
- (6) Oreg, Y.; Refael, G.; von Oppen, F. Helical Liquids and Majorana Bound States in Quantum Wires. *Phys. Rev. Lett.* **2010**, *105*, 177002.
- (7) Mourik, V.; Zuo, K.; Frolov, S. M.; Plissard, S. R.; Bakkers, E. P. A. M.; Kouwenhoven, L. P. Signatures of Majorana Fermions in Hybrid Superconductor-Semiconductor Nanowire Devices. *Science* **2012**, *336*, 1003–1007.
- (8) Das, A.; Ronen, Y.; Most, Y.; Oreg, Y.; Heiblum, M.; Shtrikman, H. Zero-Bias Peaks and Splitting in an Al–InAs Nanowire Topological Superconductor as a Signature of Majorana Fermions. *Nat. Phys.* **2012**, *8*, 887–895.
- (9) Deng, M. T.; Yu, C. L.; Huang, G. Y.; Larsson, M.; Caroff, P.; Xu, H. Q. Anomalous Zero-Bias Conductance Peak in a Nb–InSb Nanowire–Nb Hybrid Device. *Nano Lett.* **2012**, *12*, 6414–6419.
- (10) Churchill, H. O. H.; Fatemi, V.; Grove-Rasmussen, K.; Deng, M. T.; Caroff, P.; Xu, H. Q.; Marcus, C. M. Superconductor-Nanowire Devices from Tunneling to the Multichannel Regime: Zero-Bias Oscillations and Magnetoconductance Crossover. *Phys. Rev. B: Condens. Matter Mater. Phys.* **2013**, *87*, 241401.
- (11) Takei, S.; Fregoso, B. M.; Hui, H. Y.; Lobos, A. M.; Das Sarma, S. Soft Superconducting Gap in Semiconductor Majorana Nanowires. *Phys. Rev. Lett.* **2013**, *110*, 186803.
- (12) Krogstrup, P.; Ziino, N. L. B.; Albrecht, S. M.; Madsen, M. H.; Johnson, E.; Nygard, J.; Marcus, C. M.; Jespersen, T. S.; Chang, W. Epitaxy of Semiconductor-Superconductor Nanowires. *Nat. Mater.* **2015**, *14*, 400–406.
- (13) Gazibegovic, S.; Car, D.; Zhang, H.; Balk, S. C.; Logan, J. A.; de Moor, M. W. A.; Cassidy, M. C.; Schmits, R.; Xu, D.; Wang, G.; Krogstrup, P.; Op het Veld, R. M. L.; Zuo, K.; Vos, Y.; Shen, J.; Bouman, D.; Shojaei, B.; Pennachio, D.; Lee, J. S.; van Veldhoven, J. S.; Koelling, S.; Verheijen, M. A.; Kouwenhoven, L. P.; Palmstrøm, C.

J.; Bakkers, E. P. A. M. Epitaxy of Advanced Quantum Nanowire Devices. *Nature* **2017**, *548*, 434–438.

- (14) Gül, Ö.; Zhang, H.; de Vries, F. K.; van Veen, J.; Zuo, K.; Mourik, V.; Conesa-Boj, S.; Nowak, M. P.; van Woerkom, D. J.; Quintero-Pérez, M.; Cassidy, M. C.; Geresdi, A.; Kölling, S.; Car, D.; Plissard, S. R.; Bakkers, E. P. A. M.; Kouwenhoven, L. P. Hard Superconducting Gap in InSb Nanowires. *Nano Lett.* **2017**, *17*, 2690–2696.
- (15) Zhang, H.; Gül, Ö.; Conesa-Boj, S.; Nowak, M. P.; Wimmer, M.; Zuo, K.; Mourik, V.; de Vries, F. K.; van Veen, J.; de Moor, M. W. A.; Bommer, J. D. S.; van Woerkom, D. J.; Car, D.; Plissard, S. R.; Bakkers, E. P. A. M.; Quintero-Pérez, M.; Cassidy, M. C.; Koelling, S.; Goswami, S.; Watanabe, K.; Taniguchi, T.; Kouwenhoven, L. P. Ballistic Superconductivity in Semiconductor Nanowires. *Nat. Commun.* 2017, 8, 16025.
- (16) Driessen, E. F. C.; Coumou, P.; Tromp, R. R.; De Visser, P. J.; Klapwijk, T. M. Strongly Disordered TiN and NbTiN s-wave Superconductors Probed by Microwave Electrodynamics. *Phys. Rev. Lett.* **2012**, *109*, 107003.
- (17) Liu, C. X.; Sau, J. D.; Das Sarma, S. Role of Dissipation in Realistic Majorana Nanowires. *Phys. Rev. B: Condens. Matter Mater. Phys.* **2017**, 95, 054502.
- (18) Deng, M. T.; Vaitiekėnas, S.; Hansen, E. B.; Danon, J.; Leijnse, M.; Flensberg, K.; Nygård, J.; Krogstrup, P.; Marcus, C. M. Majorana Bound State in a Coupled Quantum-Dot Hybrid-Nanowire System. *Science* **2016**, 354, 1557–1562.
- (19) Meservey, R.; Tedrow, P. Properties of very thin aluminum films. J. Appl. Phys. 1971, 42, 51.
- (20) Friedl, M.; Cerveny, K.; Weigele, P.; Tütüncüoglu, G.; Martí-Sánchez, S.; Huang, C.; Patlatiuk, T.; Potts, H.; Sun, Z.; Hill, M. O.; Güniat, L.; Kim, W.; Zamani, M.; Dubrovskii, V. M.; Arbiol, J.; Lauhon, L. J.; Zumbühl, D. M.; Fontcuberta i Morral, A. Template-Assisted Nanowire Networks for Scalable Topological Quantum Computing Schemes. *Nano Lett.* **2018**, *18*, 2666–2671.
- (21) Suyatin, D. B.; Thelander, C.; Björk, M. T.; Maximov, I.; Samuelson, L. Sulfur Passivation for Ohmic Contact Formation to InAs Nanowires. *Nanotechnology* **2007**, *18*, 105307.
- (22) Janvier, C.; Tosi, L.; Bretheau, L.; Girit, Ç. Ö.; Stern, M.; Bertet, P.; Joyez, P.; Vion, D.; Esteve, D.; Goffman, M. F.; Pothier, H.; Urbina, C. Coherent Manipulation of Andreev States in Superconducting Atomic Contacts. *Science* **2015**, 349, 1199–1202.
- (23) Larsen, T. W.; Petersson, K. D.; Kuemmeth, F.; Jespersen, T. S.; Krogstrup, P.; Nygård, J.; Marcus, C. M. Semiconductor-Nanowire-Based Superconducting Qubit. *Phys. Rev. Lett.* **2015**, *115*, 127001.
- (24) Kang, J. H.; Grivnin, A.; Bor, E.; Reiner, J.; Avraham, N.; Ronen, Y.; Cohen, Y.; Kacman, P.; Shtrikman, H.; Beidenkopf, H. Robust Epitaxial Al Coating of Reclined InAs Nanowires. *Nano Lett.* **2017**, *17*, 7520–7527.
- (25) Beenakker, C. W. J. Quantum Transport in Semiconductor-Superconductor Microjunctions. *Phys. Rev. B: Condens. Matter Mater. Phys.* **1992**, *46*, 12841.
- (26) Chang, W.; Albrecht, S. M.; Jespersen, T. S.; Kuemmeth, F.; Krogstrup, P.; Nygård, J.; Marcus, C. M. Hard Gap in Epitaxial Semiconductor-Superconductor Nanowires. *Nat. Nanotechnol.* **2015**, 10, 232–236.
- (27) Gill, S. T.; Damasco, J.; Car, D.; Bakkers, E. P. A M.; Mason, N. Hybrid Superconductor-Quantum Point Contact Devices using InSb Nanowires. *Appl. Phys. Lett.* **2016**, *109*, 233502.
- (28) Blonder, G. E.; Tinkham, M.; Klapwijk, T. M. Transition from Metallic to Tunneling Regimes in Superconducting Microconstrictions: Excess Current, Charge Imbalance, and Supercurrent Conversion. *Phys. Rev. B: Condens. Matter Mater. Phys.* **1982**, 25, 4515.
- (29) Octavio, M.; Tinkham, M.; Blonder, G. E.; Klapwijk, T. M. Subharmonic Energy-Gap Structure in Superconducting Constrictions. *Phys. Rev. B: Condens. Matter Mater. Phys.* **1983**, *27*, 6739.
- (30) Averin, D.; Bardas, A. ac Josephson Effect in a Single Quantum Channel. *Phys. Rev. Lett.* **1995**, *75*, 1831.

(31) Cuevas, J. C.; Martín-Rodero, A.; Yeyati, A. L. Hamiltonian Approach to the Transport Properties of Superconducting Quantum Point Contacts. *Phys. Rev. B: Condens. Matter Mater. Phys.* **1996**, *54*, 7366.

- (32) Kjaergaard, M.; Nichele, F.; Suominen, H. J.; Nowak, M. P.; Wimmer, M.; Akhmerov, A. R.; Folk, J. A.; Flensberg, K.; Shabani, J.; Palmstrøm, C. J.; Marcus, C. M. Quantized Conductance Doubling and Hard Gap in a Two-Dimensional Semiconductor—Superconductor Heterostructure. *Nat. Commun.* **2016**, *7*, 12841.
- (33) Goffman, M. F.; Cron, R.; Levy Yeyati, A.; Joyez, P.; Devoret, M. H.; Esteve, D.; Urbina, C. Supercurrent in Atomic Point Contacts and Andreev States. *Phys. Rev. Lett.* **2000**, *85*, 170.
- (34) Vion, D.; Gotz, M.; Joyez, P.; Esteve, D.; Devoret, M. H. Thermal Activation above a Dissipation Barrier: Switching of a Small Josephson Junction. *Phys. Rev. Lett.* **1996**, *77*, 3435.
- (35) Winkelmann, C. B.; Roch, N.; Wernsdorfer, W.; Bouchiat, V.; Balestro, F. Superconductivity in a Single-C60 Transistor. *Nat. Phys.* **2009**, *5*, 876–879.
- (36) Gallagher, P.; Lee, M.; Williams, J. R.; Goldhaber-Gordon, D. Gate-Tunable Superconducting Weak Link and Quantum Point Contact Spectroscopy on a Strontium Titanate Surface. *Nat. Phys.* **2014**, *10*, 748.
- (37) Beenakker, C. W. J.; van Houten, J. Current through a Superconducting Quantum Point Contact Shorter than the Coherence Length. *Phys. Rev. Lett.* **1991**, *66*, 3056.
- (38) Abay, S.; Persson, D.; Nilsson, H.; Xu, H. Q.; Fogelström, M.; Shumeiko, V.; Delsing, P. Quantized Conductance and its Correlation to the Supercurrent in a Nanowire Connected to Superconductors. *Nano Lett.* **2013**, *13*, 3614–3617.
- (39) Courtois, H.; Meschke, M.; Peltonen, J. T.; Pekola, J. P. Origin of Hysteresis in a Proximity Josephson Junction. *Phys. Rev. Lett.* **2008**, *101*, 067002.
- (40) Higginbotham, A. P.; Albrecht, S. M.; Kirsanskas, G.; Chang, W.; Kuemmeth, F.; Krogstrup, P.; Jespersen, T. S.; Nygard, J.; Flensberg, K.; Marcus, C. M. Parity Lifetime of Bound States in a Proximitized Semiconductor Nanowire. *Nat. Phys.* **2015**, *11*, 1017–1021
- (41) Albrecht, S. M.; Higginbotham, A. P.; Madsen, M.; Kuemmeth, F.; Jespersen, T. S.; Nygård, J.; Krogstrup, P.; Marcus, C. M. Exponential Protection of Zero Modes in Majorana Islands. *Nature* **2016**, 531, 206–209.
- (42) Buttiker, M. Role of Quantum Coherence in Series Resistors. *Phys. Rev. B: Condens. Matter Mater. Phys.* **1986**, 33, 3020.
- (43) Kane, B. E.; Facer, G. R.; Dzurak, A. S.; Lumpkin, N. E.; Clark, R. G.; Pfeiffer, L. N.; West, K. W. Quantized Conductance in Quantum Wires with Gate-Controlled Width and Electron Density. *Appl. Phys. Lett.* **1998**, 72, 3506.
- (44) Scheller, C. P.; Liu, T.-M.; Barak, G.; Yacoby, A.; Pfeiffer, L. N.; West, K. W.; Zumbühl, D. M. Possible Evidence for Helical Nuclear Spin Order in GaAs Quantum Wires. *Phys. Rev. Lett.* **2014**, *112*, 066801.
- (45) Csonka, S.; Hofstetter, L.; Freitag, F.; Oberholzer, S.; Schönenberger, C.; Jespersen, T. S.; Aagesen, M.; Nygård, J. Giant Fluctuations and Gate Control of the g-Factor in InAs Nanowire Quantum Dots. *Nano Lett.* **2008**, *8*, 3932–3935.
- (46) Schroer, M. D.; Petersson, K. D.; Jung, M.; Petta, J. R. Field Tuning the g-Factor in InAs Nanowire Double Quantum Dots. *Phys. Rev. Lett.* **2011**, *107*, 176811.
- (47) Lee, E. J. H.; Jiang, X.; Houzet, M.; Aguado, R.; Lieber, C. M.; De Franceschi, S. Spin-Resolved Andreev Levels and Parity Crossings in Hybrid Superconductor—Semiconductor Nanostructures. *Nat. Nanotechnol.* **2014**, *9*, 79—84.
- (48) Kretinin, A. V.; Popovitz-Biro, R.; Mahalu, D.; Shtrikman, H. Multimode Fabry-Pérot Conductance Oscillations in Suspended Stacking-Faults-Free InAs Nanowires. *Nano Lett.* **2010**, *10*, 3439–3445
- (49) Kammhuber, J.; Cassidy, M. C.; Zhang, H.; Gül, Ö.; Pei, F.; de Moor, M. W. A.; Nijholt, B.; Watanabe, K.; Taniguchi, T.; Car, D.; Plissard, S. R.; Bakkers, E. P. A. M.; Kouwenhoven, L. P. Conductance

Quantization at Zero Magnetic Field in InSb Nanowires. *Nano Lett.* **2016**, *16*, 3482–3486.

- (50) Wimmer, M.; Akhmerov, A. R.; Dahlhaus, J. P.; Beenakker, C. W. J. Quantum Point Contact as a Probe of a Topological Superconductor. *New J. Phys.* **2011**, *13*, 053016.
- (51) Zhang, H.; Liu, C.-X.; Gazibegovic, S.; Xu, D.; Logan, J. A.; Wang, G.; van Loo, N.; Bommer, J. D. S.; De Moor, M. W. A.; Car, D.; Op het Veld, R. L. M.; et al. Quantized Majorana Conductance. *Nature* 2018, 556, 74–79.